LUMION: Fast Fault Recovery for ML Jobs Using Programmable Optical Fabrics

Abhishek Vijaya Kumar* Cornell University
Eric Ding Cornell University
Arjun Devraj Cornell University
Darius Bunandar Lightmatter
Rachee Singh Cornell University

Abstract

When accelerators fail in modern ML datacenters, operators migrate the affected ML training or inference jobs to entirely new racks. This approach, while preserving network performance, is highly inefficient, requiring datacenters to reserve full racks of idle accelerators for fault tolerance. In this paper, we address this resource inefficiency by introducing LUMION, a novel reconfigurable optical fabric for connecting accelerators within a datacenter rack. Instead of migrating entire ML jobs, LUMION dynamically integrates spare accelerators into ongoing workloads as failures occur, thereby maintaining consistent performance without costly migrations. We show the benefits of LUMION by building an end-to-end hardware prototype. Our experiments fine-tune Llama 3.2 and show that LUMION swaps a failed GPU with a healthy one and restarts the ML job within ≈ 1 second of the failure. LUMION achieves higher inter-GPU bandwidth compared to traditional electrical racks after replacing failed accelerators with spare ones, leading to nearly $2\times$ improvement in fine-tuning throughput.

1 Introduction

Recent years have seen the deployment of ML-centric datacenters *i.e.,* datacenters that are optimized for the computation and communication needs of large-scale distributed ML workloads [1–3]. These datacenters connect ML accelerators (*e.g.,* GPUs, TPUs) with high bandwidth links in a rack. Several racks are connected using lower bandwidth links to form the entire ML datacenter. For instance, in the popular Google TPU datacenter, a rack consists of 64 TPUs connected in the shape of a torus; 64 such racks form the full TPU datacenter with $64 \times 64 = 4,096$ TPUs [1].

Large-scale ML training jobs require thousands of accelerators for weeks at a time, making hardware failures inevitable at this massive scale. For example, it took Meta several weeks to train their 405B-parameter language model in a 16,000-GPU datacenter. Approximately half of all interruptions during this process were due to GPU failures [4]. Each accelerator failure can stall the entire training job. Therefore, datacenter operators use various strategies to mitigate these incidents, like reserving spare accelerators that can be hot-swapped into the ML job when an accelerator fails.

When a failed accelerator is replaced by a healthy one, it is essential that the updated set of accelerators assigned to the ML job does not experience degraded network performance relative to the original allocation before the failure. Preserving network performance is crucial since distributed ML workloads rely on the bandwidth available for communication between accelerators. Reduced bandwidth translates to lower inference and training throughput (§2).

*correspondence to abhishek@cs.cornell.edu

Preprint. Under review.

However, preserving network performance after an accelerator failure is challenging. If the replacement accelerator resides in a different rack, inter-accelerator traffic of the ML job must now traverse slower inter-rack links. Even if the new accelerator is in the same rack, integrating it into the existing allocation can cause network congestion — a scenario when multiple accelerators compete for shared network resources, reducing the available bandwidth for each accelerator.

A common solution to this problem is to migrate the entire ML job from the rack with the failed accelerator to another fully functional rack in the datacenter. In fact, Google's TPU datacenters use this approach [1]. This solution is effective in preserving network performance since the ML job is migrated to an unused rack with similar network characteristics as the original one. However, it incurs significant resource inefficiency. In the worst case, managing just one accelerator failure requires having an entire spare rack available, translating to $64\times$ resource over-provisioning.

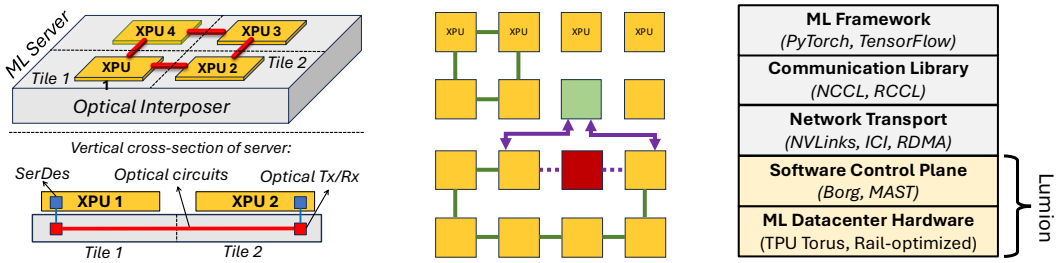

(a) Accelerators on LUMION tiles. (b) Hot-swapping XPU. (c) End-to-end ML stack.

Figure 1: 1a(top) shows how ML accelerators (XPUs) are stacked on top the optical interposer, LUMION. Connections between accelerators are direct optical links. 1a(bottom) shows a vertical cross-section of the server where two 2 XPUs connect on two tiles and communicate via the underlying optical link (shown in red). 1b shows how links can be programmed (dashed links $\rightarrow$ to purple arrows) when failures occur (red) to hot-swap a free accelerator (green). 1c shows how LUMION is modifying the lower-most layers of the ML stack.

1.1 Our contributions: programmable optical fabrics in GPU racks

State-of-the-art ML datacenters achieve consistent network performance after accelerator failures by massively over-provisioning accelerators, leading to resource under-utilization and inefficiency [1]. In this work, we address this challenge by developing a new kind of network, LUMION, to connect accelerators in the rack of an ML datacenter. LUMION connects accelerators in a rack using optical links, instead of the traditional electrical ones (*e.g.,* NVlinks [5], ICI [1], PCIe [6]).

LUMION's optical links have two properties that ensure the network performance of an ML job is preserved after replacing a failed accelerator. **First**, each optical connection in LUMION is dedicated to only one pair of accelerators in the rack, meaning that there can be no congestion since only one pair of accelerators is using that link. This is in contrast to traditional electrical connections in the racks of ML datacenters, where multiple pairs of accelerators can send data on the same network link, causing congestion. **Second**, LUMION can create these optical connections on-demand between existing and spare accelerators once a failure occurs. These two properties allow LUMION to hot-swap a healthy accelerator located in the same rack without having to migrate the job to a different rack, while preserving the network performance of the ML job.

In LUMION's hardware architecture, accelerators in an ML server are mounted on an *optical interposer* [7, 8]. The interposer is a substrate that implements optical connections between accelerators stacked on top of it. Figure 1a shows LUMION's architecture of an ML server with ML accelerators stacked on the optical interposer. Figure 1b shows an example configuration of optical connections between accelerators stacked on LUMION. Overall, we make the following contributions in this work:

- **An optical fabric for ML datacenters.** We build a programmable optical fabric, LUMION, to connect accelerators in a rack. LUMION can create on-demand direct optical links to connect accelerators in the same rack, allowing them to communicate without network congestion (§3).
- **A system for replacing failed accelerators at run time.** We develop a software system that leverages the LUMION optical fabric to connect existing and spare accelerators once a failure occurs. LUMION ensures that the replacement accelerator can be used in the ML job without causing network congestion and migrating the ML job to a different rack is no longer necessary. LUMION can swap a failed accelerator and restart the ML job within ≈ 1 second (§4).

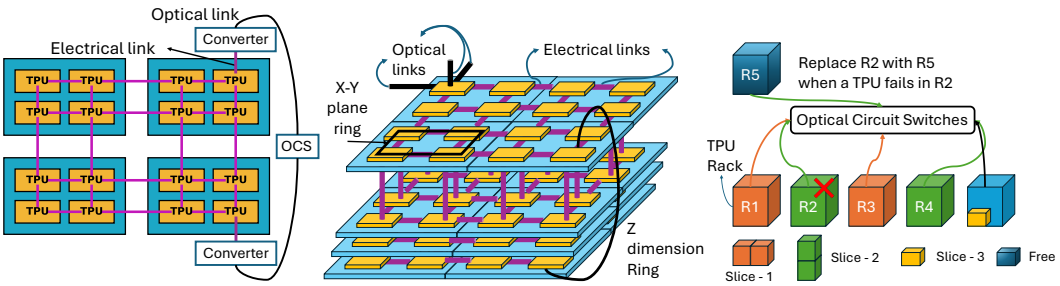

(a) TPU plane. (b) TPU rack. (c) Scale-out connections.

Figure 2: 2a shows a horizontal *plane* of the TPU rack. This plane has 4 servers (in blue), each with 4 TPU chips (in yellow). Each TPU chip has its escape bandwidth divided across links in three directions: X, Y and Z. 2b shows how multiple planes are connected to each other to form a rack. Figures 2a, 2b show the different rings used by the collective communication algorithms optimized for the torus topology. Figure 2c shows how racks are connected to each other via OCSes to allocate multi-rack and sub-rack TPU slices to tenants.

- **End-to-end hardware prototype.** We build an end-to-end hardware prototype of LUMION's hardware and software to connect four GPUs in a rack. Using the prototype, we show a series GPU failure scenarios in which LUMION achieves optimal bandwidth between accelerators, resulting in nearly 2× faster collective communication and ML throughput (§5).

2 The conundrum of fault tolerance in modern ML datacenters

Cloud providers are deploying ML datacenters with thousands of accelerators to satisfy the rapidly growing demands of large-scale ML workloads [1, 9, 4]. At this massive scale, accelerator hardware failures are frequent and inevitable. For example, during Meta's training of the 405B-parameter Llama model across 16,000 GPUs, approximately 50% of all interruptions resulted from GPU hardware failures, averaging roughly one failure every two hours [4]. Each such accelerator failure can stall entire ML training or inference jobs, making it crucial to manage accelerator failures.

However, managing accelerator failures effectively introduces a fundamental tension: preserving ML job performance after failures requires either massive hardware over-provisioning or tolerating significant network congestion. Massive over-provisioning results in inefficient hardware utilization, whereas network congestion severely impacts ML job performance. In fact, reduced bandwidth due to network congestion can degrade the performance of ML jobs by as much as 50% (Figures 3b, 3c). This section elaborates on this tension, using Google's TPU datacenter architecture as a representative example due to its detailed documentation and widespread use for large-scale ML [1, 2, 10, 11].

2.1 Network connectivity in modern ML datacenters

ML models are growing rapidly, becoming too large for a single accelerator's memory. This growth necessitates distributed training and inference, where multiple accelerators collaboratively train or serve a model. Communication among accelerators during distributed ML happens through a set of well-defined patterns known as collective communication primitives (*e.g.,* ALLREDUCE) [12, 13]. Because accelerators often remain idle during these communication steps, minimizing communication latency directly translates into improved hardware utilization and faster job completion.

To address these communication challenges, modern ML datacenters such as Google's TPU datacenters adopt specialized network architectures called *direct-connect* fabrics. In these designs, pairs of accelerators can communicate via direct links without intermediate *packet-switching* [1].

Scale-up domains: racks of accelerators. Google's TPU datacenter consists of 64 racks, also called *scale-up domains*, each containing 64 TPUs. Each rack has 16 servers (Figure 2b) where each server has 4 TPUs interconnected using copper-based electrical links called inter-chip interconnect (ICI) (pink links in Figure 2a). Accelerators in these racks are arranged in a 3D torus topology with wrap-around links of the torus (black optical links in Figure 2a) being fiber-based optical connections.

Scale-out domains: interconnecting multiple racks. A *scale-out domain* connects all 64 racks together, creating the full datacenter of 4,096 TPUs (Figure 2b). Each rack is a 3D torus, easily visualized as a cube with 6 faces, each face housing 16 TPUs. TPUs located at corresponding positions across racks connect to optical circuit switches (OCSes) to implement inter-rack communication

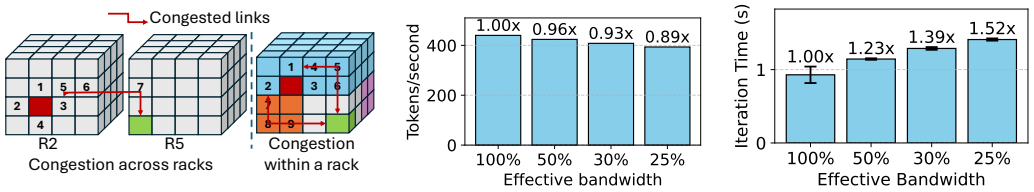

(a) Chip granularity. (b) vLLM, Yi-34B. (c) Llama 1B, training.

Figure 3: Figure 3a (left) shows that replacing the failed TPU in R2 with an idle TPU from R4 introduces network congestion along TPUs 5, 6, and 7. The right side of Figure 3a highlights how allocating multiple slices in the same rack (shown in different colors) leads to congestion. In 3b we execute Yi-34B for inference using vLLM with a tensor parallel degree of 2. In 3c, we finetune Llama 2 with 8 layers and 16 attention heads with Tensor parallelism. We executed both of these experiments on 2 NvLinked A100 GPUs.

(Figure 2b). We note that the intra-rack connectivity uses copper-based electrical links, while the inter-rack connectivity uses fiber-based optical links.

Tenant slices. A slice is a subset of TPUs allocated to a cloud tenant (Figure 2c). Slice sizes range from a fraction of a rack ($<$ 64 TPUs) to multiple racks ($>$ 64 TPUs). Cloud provider allocates multi-rack slices by programming the OCSes to connect racks in different positions in the desired shape (*e.g.,* , Slice-1, 2 in Figure 2c). Slice allocations in the TPU datacenter must adhere to the dimensions and connectivity of a torus ($i \times j \times k$) [14]. Tenants deploy their training and inference jobs on the allocated TPU slice. During the job's lifetime, collective communication primitives are executed over the slice to support data, model, pipeline parallelisms.

Collective communication in TPU datacenters. While there are many algorithms for collective communication primitives [15, 12, 16], some are better suited for the TPU direct-connect topology than others. For the AllReduce collective, multi-dimensional bucket ring algorithm [17–19] is well-suited for the direct-connect fabric in TPU datacenters (Figure 2b). This algorithm orchestrates accelerator communication in logical rings along each dimension (X, Y, and Z axes) of the 3D torus topology. Each accelerator communicates only with its immediate neighbors along each dimension, thereby avoiding congestion on links. However, the overall throughput of these communication rings depends on the bandwidth of the slowest link (Figure 2). Thus, ensuring consistent link bandwidth across the entire topology becomes essential to take advantage of the direct-connect fabric.

2.2 Handling accelerator failures: trade-offs in fault tolerance

When an accelerator allocated to a tenant slice fails, the ML job running on that slice stalls. To minimize downtime, datacenter operators attempt to quickly replace the failed accelerator with a spare and restart the job. However, integrating this spare accelerator into the existing slice can degrade the performance of the network connecting the accelerators. This occurs since communication paths between existing and spare accelerators must be routed over links that are already used for collective communication primitives of different slices. This can cause congestion on shared network links. Figure 3a shows how adding a replacement accelerator introduces new communication paths that overlap on existing routes within the rack, resulting in congestion. Congestion reduces the available bandwidth, negatively affecting the performance of both the impacted ML job and any other workloads sharing the affected network links.

To quantify the performance impact of reduced network bandwidth on ML tasks, we conduct controlled experiments. Since cloud providers do not allow us to modify the network bandwidth in their scale-up domains, we simulate bandwidth reduction due to network congestion by increasing the sizes of communication buffers involved in collective operations without altering compute tasks. Because the effective communication cost is proportional to buffer size and inversely proportional to network bandwidth, adjusting buffer sizes effectively mimics bandwidth reduction. As shown in Figure 3b, this artificial bandwidth reduction results in over a 10% drop in inference throughput for a 34B-parameter Yi model [20]. Similarly, Figure 3c shows that it leads to more than a 50% increase in iteration time during full fine-tuning of the Llama-3.2 1B model. These results highlight how even modest reductions in network bandwidth can significantly impair ML workload performance.

A alternate approach, used by Google's TPU datacenters [2], is to handle failures by migrating the entire ML job away from the rack containing the failed accelerator to a fully operational spare rack. As shown in Figure 2c, even a single accelerator failure necessitates reserving an entire unused rack.

This results in extreme hardware over-provisioning of up to $64\times$. While this approach guarantees consistent network performance before and after accelerator failures, it incurs substantial resource inefficiency and under-utilization, preventing these spare resources from supporting other workloads.

Ultimately, current ML datacenters face a conundrum: achieving fault tolerance either comes at the high cost of massive hardware over-provisioning or risks severe performance degradation due to network congestion. Addressing this tension is critical to designing scalable and efficient ML datacenters. The next section introduces LUMION, our novel approach that resolves this fundamental trade-off using reconfigurable optical fabrics to provide both fault tolerance and resource efficiency.

3 Programmable optical networks in the datacenter rack

We address the challenge of fault tolerance in ML datacenters by developing a novel network technology and architecture to connect accelerators in the rack, called LUMION. We describe the low-level details of the LUMION hardware in Appendix but explain how it addresses the challenge.

In the LUMION architecture, accelerators in a server are stacked onto an optical substrate known as an *optical interposer* (see Figure 1a). This interposer contains a dense mesh of optical waveguides *i.e.,* tiny channels that guide light signals, and programmable switches. Each accelerator connects electrically to optical transmitters and receivers embedded on the interposer, converting electrical signals into optical ones. Data travels through direct optical connections formed by configuring the optical switches on the interposer. These direct connections eliminate network congestion because each link exclusively serves one accelerator pair.

One LUMION server connects to others servers using attached optical fibers. Waveguides leaving a tile at the edge of LUMION feed signals into fibers. Using attached fibers, we cascade several LUMION servers to create rack-scale accelerator deployments [21]. Our experiments show that signal propagation loss in waveguides and the loss while crossing a tile on LUMION is low, allowing us to create optical connections between accelerators in different servers of the same rack.

The critical advantage of this programmable optical network within the rack is its ability to instantly (within microseconds) reroute communication paths around failed accelerators.

What changes in the TPU datacenter with LUMION? With LUMION there will be no more copper-based electrical ICI connections (pink lines in Figure 2b) between TPUs within a rack. LUMION re-creates the same torus topology within each rack by programming the optical interposer. The optical connections between TPUs within the same server travels through the waveguides. The optical connections between TPUs across servers travels through fibers between servers in addition to traveling trough waveguides. LUMION directly connects the fibers leaving the server to the OCSes. LUMION accommodates all the additional optical connections required during fault tolerance on different waveguides and fibers. This provides each optical connection a dedicated end-to-end physical path which eliminates congestion. Consequently, accelerator failures only minimally disrupt the ML workload, reducing downtime from minutes or even hours to approximately one second.

Can electrical packet switches address the challenges LUMION addresses? One might argue that connecting accelerators within the server using an *ideal packet switch* (*e.g.,* NVSwitch [22, 5]) can achieve the same effect: congestion-free connections between all accelerators [23, 24]. However, inter-accelerator bandwidth within modern servers is already massive — over 300 gigabytes per second in one direction [22]— making it harder to stay true to the ideal switch abstraction. This has already resulted in evidence of congestion in switched server-scale interconnects [25, 12].

4 In-place fault tolerance with LUMION

We design a *fault manager* in LUMION to tolerate faults without hardware overprovisioning or inducing network congestion. To achieve this, we must answer the following research questions:

- **How many TPUs to add?** To prevent overprovisioning of TPUs, it is essential to precisely determine the number of additional TPUs required for fault tolerance.
- **Where to add the spare TPUs?** The new optical connections required for fault tolerance must be routed over distinct fibers to preserve signal integrity and avoid congestion, often requiring adding more fibers to the rack. Therefore, it is crucial to place spare TPUs such that it reduces the number of new fibers needed in each rack. Note that we add TPUs instead of reserving existing ones to preserve the rack's original dimensions. Reserving a server—for example, anywhere within a rack,

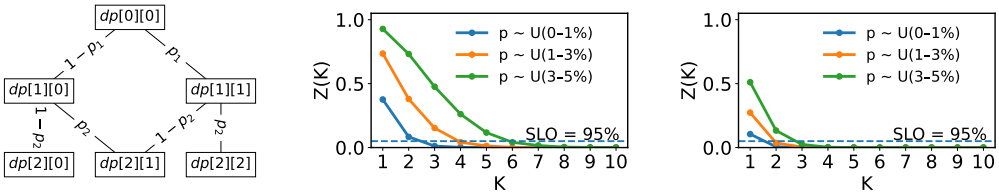

(a) Tree of dp matrix. (b) SRG = TPU (c) SRG = Server with 4 TPUs

Figure 4: Figure 4a shows the recursion tree of Z(K) for 2 SRGs. In Figure 4b, we set SRG to a single TPU and N to 64. shows that with 4 TPUs are sufficient to respect 95% SLO when SRG is a single TPU. Similarly Figure 4c shows that two additional servers (4 TPUs per server) are sufficient to respect 95% SLO in most cases. In both, 4b and 4c, additional hardware requirement increases with increase in failure probability distribution

reduces the effective size of the rack (e.g., from $(4 \times 4 \times 4)$ to $(4 \times 4 \times 3)$ if we reserve a corner server), which breaks support for multi-rack slices with sizes that are multiples of $(4 \times 4 \times 4)$.

- **How to route on the interposer?** Every optical connection needs to be routed through optical interposer mesh — a massive graph with thousands of waveguides. Each connection should be on a distinct set of waveguides to maintain signal integrity and avoid congestion. This requires a routing algorithm that finds non-overlapping paths while scaling to thousands of nodes.

How many TPUs can fail simultaneously? The number of TPUs to add is upper bounded by the number of TPUs that can simultaneously fail. We find the optimal number of TPUs by determining the highest number of TPUs that can fail within a given Service Level Objective (SLO). *e.g.,* for an SLO of 95%, we need enough free TPUs to tolerate failure scenarios with a probability > 5%.

Shared risk groups (SRG). Components in a datacenter follow the fate-sharing principle [26] which suggests that related parts of a system fail together or none of them fail. We use the popular concept of a Shared Risk Group (SRG), a group of resources that fail together. Each SRG fails independently of others since each SRG consists of any resources that have shared dependencies (aside from datacenter-wide failures). For instance, if a TPU's compute cores or memory fail, the entire TPU is treated as failed. Similarly, a failure in a server's power supply, host CPU, or DRAM results in the failure of the entire server, including all the TPUs it hosts.

Failure probability of a SRG. We define the probability of failure of a SRG as $P_{\text{fail}} = \frac{T_{\text{repair}}}{T_{\text{active}}+T_{\text{repair}}}$ where T_{repair} is the duration when the SRG is faulty including the time taken to repair it, T_{active} is the duration of time when the SRG is healthy. This duration should be extracted from the logging, telemetry and diagnostic collection pipeline of the cloud provider.

Probability of K or more failures. We define $Z(K)$ as the probability that at least K SRGs fail in N SRGs. Let p_i be the P_{fail} of the i^{th} SRG, then $Z(K)$ is given by Equation $Z(K) = \sum_{i=K}^{N} \sum_{\substack{A \subseteq \{1,\ldots,N\} \\ |A|=i}} \left[\prod_{j \in A} p_j\right] \left[\prod_{j \notin A} (1-p_j)\right]$. $Z(K)$ is expensive to compute as it iterates over all possible subsets of sizes from K to N.

Key insight: Our key insight is that the inner sum of $Z(K)$ can be represented as a recursive relation with smaller sub-problems. Let $dp[i][k]$ be the probability of k failures in i SRGs, then the recursive relation is given by $dp[i][k] = dp[i-1][k-1] * (p_i) + dp[i-1][k] * (1-p_i)$. We formulate this as a dynamic program which computes larger dps using smaller solutions as shown in Figure 4a. Given the dp matrix, we can compute Z(K) by summing over all probabilities where at least K failures occur, i.e., $Z(K) = \sum_{k=K}^{N} dp[N][k]$. This reduces the computational complexity from $O(2^N)$ to polynomial $O(N^2)$, making it tractable for large networks with many SRGs. We pick K SRGs such that $Z(K) \leq (1-S)$ where S is $\frac{SLO}{100}$. This K guarantees that the probability of K or more SRGs failing is less than $(1-S)$. So, all the failures that occur during the remaining S fraction of the time can be gracefully handled by adding K more SRGs.

How do we pick N? We calculate $Z(K)$ at the rack granularity because adding more TPUs not only requires adding more compute but also networking resources to connect these TPUs to the existing TPUs. One can connect additional TPUs to the OCSes and replace failed TPUs in any rack by the additional TPUs. However, the ports on the OCSes connecting multiple racks are already saturated which makes connecting additional TPUs to the OCSes infeasible. Cascading multiple OCSes to increase the switch radix is also challenging [2] due to optical losses. In Figure 4b, we set $N = 64$

(the number of TPUs in a rack), SRG to a single TPU and sample the failure probabilities of each TPU from three different ranges. The plot shows that reserving just 4 TPUs handles more than 95% of the failures in many cases. We also set SRG to an entire server with 4 TPUs and calculate $Z(K)$ in Figure 4c which shows that 2 servers are sufficient to handle most failures in each rack.

Placing the additional TPUs. We analyze the placement of additional TPUs by setting SRG to a single TPU. Given that a server contains four TPUs—sufficient for handling over 95% of failures when SRG=TPU, we optimize placement at server granularity. Each rack consists of 16 servers arranged in a $(2 \times 2 \times 4)$ torus. Leveraging symmetry, the unique positions where a new server can be added are $(-1, 0, 0), (0, -1, 0), (0, 0, -1), (0, -1, 1), (-1, 0, 1)$. The main tradeoff between these placement options is the number of inter-server fibers required. When a TPU fails, it must be replaced by a working TPU on a different server, which requires optical connections to cross server boundaries. These connections having same wavelengths must be placed on different fibers to maintain signal integrity. The TPU topology includes 4 fibers between each pair of servers to support connectivity (§ 2.1). These fibers provide 4 connections in each direction, which are sufficient for collective communication within physically contiguous torus slices [17]. However, fault tolerance can create physically discontiguous slices requiring additional connections, necessitating more fibers.

Reducing additional fiber provisioning. Installing and maintaining extra fibers is operationally challenging. The fiber requirement depends on (1) the rack state — slice requests allocated to the rack, (2) which TPUs fail and (3) the position of the additional server . Since the first two are beyond the cloud provider's control, we focus on optimizing (3) to reduce fiber requirements. We need to determine the minimum number of additional fibers per rack that avoids circuit overlap—a problem that is NP-hard. To tackle this, we develop an ILP-based route-finding algorithm that minimizes congestion while routing connections for a given set of endpoints. While existing methods like K-shortest path routing can be used, they often cause unnecessary overlaps, increasing fiber usage by up to 20% (§ 5.3). Modeling all combinations of rack states, TPU failures, and server positions in the ILP would be computationally infeasible. Instead, we take an empirical approach: for each server position, we run the ILP under hundreds of randomly generated rack states, with slice allocations of varying sizes and $1 - 4$ randomly failed TPUs. We have built a TPU datacenter simulator to aid us in generating the rack and failure states and arrive at the server position $(0, -1, 1)$ that has the least fiber requirement . Our empirical method can be extended to different SRGs, *e.g.,* SRG = 1 server(Figure 4c) and failing servers instead of TPUs.

4.1 Hardware control plane

fault manager communicates with daemons running on every multi-accelerator server which report the status of processes running on the TPUs. Upon detecting failure, *fault manager* searches for a free and healthy TPU and invokes *hardware control plane* to create optical connections between the neighbors of the failed TPU and the healthy TPU to logically replace the failed TPU. Finally, it restarts the job with the latest checkpoint [27].

Routing within the MZI mesh. Every optical connection originating, terminating or passing through a server needs to be routed through that server's interposer mesh. This MZI mesh consists of 100s of 1×3 MZI switches connected by waveguides and can be modeled as a graph for path computation. Standard algorithms like Dijkstra's ($O(E + V \log V)$) can become computationally expensive for large meshes since they are $N \log N$ in the number of vertices. We reduce this complexity by merging the two adjacent MZIs connected by a single waveguide into 1 still reflecting the physical properties that connect every pair of adjacent MZI switches , thereby reducing the number of vertices by $2X$. We develop an algorithm based on Dijkstra's algorithm to find routes that do not overlap on any edge on this graph to prevent signal integrity. Our algorithm finds routes in less than 0.6 seconds for grids with up-to $65K$ MZIs (256×256 grid).

5 Hardware evaluation of LUMION

We build an end-to-end hardware prototype to evaluate LUMION. Adding accelerators to the LUMION wafer-scale interconnect (§3) would need using a semiconductor fabrication facility like TSMC [28] to stack chips on the interconnect. Semiconductor packaging at the small scale of one prototype like this incurs the cost of several million dollars, which is prohibitively expensive for academic research. We overcome this challenge using an off-the-shelf silicon photonic mesh [29, 30], IPRONICS, that uses the same MZI and waveguide technology as the prototype in Figure 1. Instead of using advanced

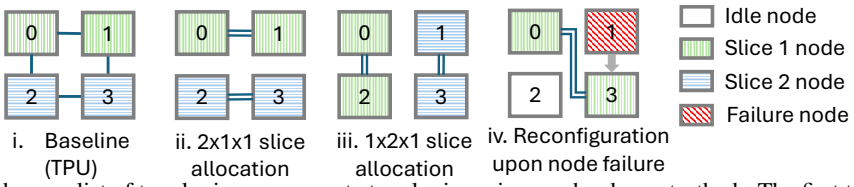

Figure 5: shows a list of topologies we generate topologies using our hardware testbed . The first topology is identical to TPU's topology but with 4 GPUs in a 2×2 grid. We use this topology as the baseline and compare it to other topologies LUMION generates during allocation (ii, iii) and fault tolerance (iv).

packaging, this mesh connects to compute endpoints by directly exposing the waveguides via fiber connectors which can communicate via optical transponders.

Testbed with GPUs. We connect four NVIDIA RTX 6000 Ada GPU servers to IPRONICS via their NICs and optical transceivers. We found an undocumented limitation of the IPRONICS mesh — it only accepts light with transverse-electric polarization. In contrast, all commodity transponders emit polarization multiplexed light. Due to this mismatch, connections between GPUs and the mesh were highly lossy. Despite the mesh's capability to carry terabits of traffic, we could only test it with 10 Gbps connections [31].

Baseline. We statically partition the two NIC ports across the X and Y dimensions in the baseline and perform no reconfigurations to model the default behavior of the electrically interconnected TPU rack. We also use the TPU's migration policy to tolerate faults in the baseline.

Workloads. To demonstrate end-to-end benefits, we fine-tune `Llama-3.2-1B` in PyTorch [32] on the wikitext [33] dataset, using the maximum batch size the GPU's memory permits and distributed data parallelism across 2 GPUs. We use shapes $2 \times 1 \times 1$ and $1 \times 2 \times 1$ in slice requests. Every slice generates Data parallel communication between the 2 GPUs that happens over the testbed.

5.1 Steady state performance with LUMION

We first evaluate the steady state performance of LUMION when there are no failures. We allocate two slices of different shapes, $2 \times 1 \times 1$ and $1 \times 2 \times 1$ (Figure 5 (ii, iii)) and measure the end-to-end iteration time of the training workload. In the baseline, we statically partition the bandwidth across the 2 dimensions in the baseline following what TPU clusters do today. For instance, of the two connections available on GPU-0, we connect 1 to GPU-1 and 1 to GPU-2. In contrast, LUMION programs the optical interposer to change the endpoints of these connections dynamically. Specifically, while allocating the slice, LUMION uses both the connections to connect the two GPUs in both the slices (blue lines in Figure 5(ii, iii)). This doubles the available bandwidth between the GPUs in each slice compared to the baseline (Figure 5(i)). Figure 6 shows that the improvement in bandwidth directly reduces the end-to-end finetuning iteration time of `Llama-3.2-1B` by $1.72\times$. This speedup is due to the lower AllReduce runtimes during gradient synchronization, enabled by the $2\times$ bandwidth resulting from LUMION.

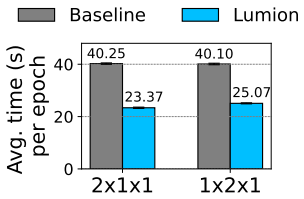

Figure 6: Iteration time.

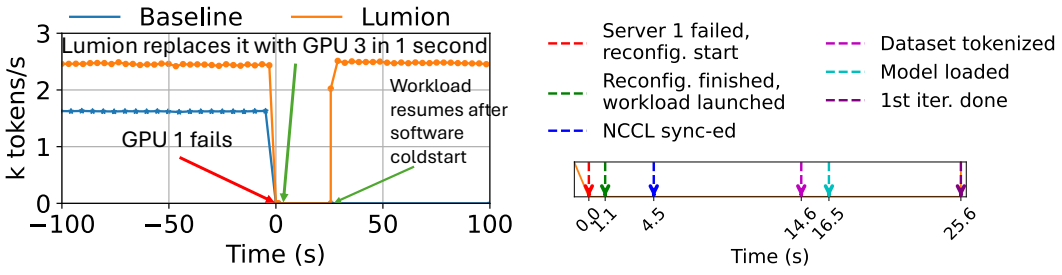

(a) Fault tolerance experiment.

(b) Zoomed-in view of Figure 7a.

Figure 7: Figures 7a and 7b (zoomed-in view of failure in 7a) show LUMION's fault handling and recovery . Workload: Llama-3.2-1B full parameter fine-tuning, wikitext-103 dataset, batch/GPU 8, DDP, 2 workers.

5.2 Fault tolerance at chip granularity

To evaluate the fault tolerance of LUMION, we simulate a hardware failure during slice 1's execution. In this experiment, we set SRG to 1 GPU and reserve GPU-3 to tolerate faults. We run the `Llama-3.2-1B` fine-tuning job on two servers (GPU-0 and GPU-1) and terminate the process on GPU-1. LUMION's *fault manager* detects the failure and reconfigures the fabric to establish connections between GPU-0 and GPU-3, enabling the workload to resume execution (Figure 5(iv)).

Figure 7a and 7b present the fault-handling timeline. The baseline suffers from 33.53% lower throughput on average due to static bandwidth partitioning and ultimately fails to complete, as no healthy accelerators remain to form a regular slice for migration. In contrast, LUMION enables continued execution by reallocating the workload to a fragmented slice. The fabric reconfiguration overhead is minimal (4.58%) compared to the cost of restarting the workload. Note that LUMION took roughly 1 second to reprogram the interposer mesh and create optical connections to *in-place patch in* the healthy GPU. Bulk of the reaction time in Figure 7b is due to software delays like moving data, model and synchronizing NCCL.

5.3 Reducing hardware underutilization during faults at large scale

We developed a TPU datacenter simulator to demonstrate the efficacy of LUMION at reducing hardware overprovisioning. Using this simulator, we fully allocate racks using publicly available production slice distribution [1] and randomly fail $1-4$ TPUs in each rack. We set SRG (§ 4) to a TPU and add 1 server (4 TPUs) at $(0,-1,1)$ in each rack to handle faults.

Baselines. We compare LUMION with the job migration policy of TPU clusters [2], which migrates the entire job, even if a single TPU fails. Additionally, we evaluate Kubernetes, a cluster management framework, using a recent policy [34] that evicts faulty-chip servers during training and replaces them with free servers having 8 accelerators in a CLOS-like topology.

Hardware underutilization. In Figure 8a, we simulate TPU failures in every rack of 16 clusters ($64 \times 16 = 1024$ racks) and measure overprovisoning. We define overprovisioning as the excess TPUs needed beyond the number of failed TPUs. For example, if 2 TPUs fail in a 32-TPU slice, the TPU baseline requires 32 replacements, resulting in an overprovisioning of $32 - 2 = 30$. Figure 8a reports the average overprovisioning with standard deviation as error bars. LUMION reduces overprovisioning by an order of magnitude compared to the TPU baseline and by $3\times$ compared to Kubernetes by creating optical connections between neighbors of failed TPUs and replacement.

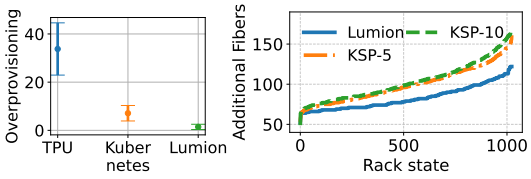

(a) Overprovisoning (b) Fiber requirement

Figure 8: Figure 8a shows the average overprovisoning over 1024 racks with standard deviation as error bars. Figure 8b shows the number of additional fibers required per rack with different routing algorithms in LUMION.

Minimizing fibers. Figure 8b shows that LUMION's algorithm (§ 4) consistently needs fewer additional fibers per rack. K shortest path (KSP) with K as 5, 10 both have up-to 30% more fiber requirement. In all our experiments, the routing algorithm (§ 4) converges to the optimal solution in less than 500 milliseconds.

6 Related work

Recent work uses optical components for failure resilience [35], capacity augmentation [36, 37] and bulk data transfers [38]. There has also been growing commercial interest in making optics an active part of routing in datacenters. For instance, Google has recently replaced the spine layer packet switches in their datacenter with optical circuit switches [1, 39, 40]. Researchers have used optics for reconfiguring the datacenter interconnects [41–44]. Researchers have used silicon photonic datacenter fabrics for improving ML training [45–49]. While optical connectivity has permeated datacenters, the interconnects between chips on compute servers remain electrical. LUMION addresses this gap.

7 Limitations and conclusion

Adoption challenges. We note that there are practical challenges that may limit large-scale adoption of optical interposers and advanced semiconductor packaging technology that LUMION relies on [50].

Ongoing research is tackling some of these challenges [51, 52]. LUMION is the first to take a step forward in this direction and show the end-to-end benefits of optical fabrics in GPU racks for ML.

Conclusion. We introduced LUMION, a novel reconfigurable optical interposer that connects accelerators within a datacenter rack. With a hardware prototype, end-to-end hardware testbed and simulation experiments, we demonstrated the benefits that optical fabrics in GPU racks promise.

Acknowledgements

This research was supported in part by ACE, one of the seven centers in JUMP 2.0, a Semiconductor Research Corporation (SRC) program sponsored by DARPA. The authors of this work are also supported by NSF Award #2444537. In addition, AVK is supported by the Cornell Bowers CIS-LinkedIn Grant and AD is supported by the NSF Graduate Research Fellowship.

References

[1] Norman P. Jouppi, George Kurian, Sheng Li, Peter Ma, Rahul Nagarajan, Lifeng Nai, Nishant Patil, Suvinay Subramanian, Andy Swing, Brian Towles, Cliff Young, Xiang Zhou, Zongwei Zhou, and David Patterson. Tpu v4: An optically reconfigurable supercomputer for machine learning with hardware support for embeddings, 2023.

[2] Yazhou Zu, Alireza Ghaffarkhah, Hoang-Vu Dang, Brian Towles, Steven Hand, Safeen Huda, Adekunle Bello, Alexander Kolbasov, Arash Rezaei, Dayou Du, Steve Lacy, Hang Wang, Aaron Wisner, Chris Lewis, and Henri Bahini. Resiliency at scale: Managing Google's TPUv4 machine learning supercomputer. In *21st USENIX Symposium on Networked Systems Design and Implementation (NSDI 24)*, pages 761–774, Santa Clara, CA, April 2024. USENIX Association. ISBN 978-1-939133-39-7. URL https://www.usenix.org/conference/nsdi24/presentation/zu.

[3] Zhenguo Wu, Liang Yuan Dai, Yuyang Wang, Songli Wang, and Keren Bergman. Flexible silicon photonic architecture for accelerating distributed deep learning. *Journal of Optical Communications and Networking*, 16(2):A157–A168, 2024. doi: 10.1364/JOCN.497372.

[4] Meta. The llama 3 herd of models, 2024. URL https://ai.meta.com/research/publications/the-llama-3-herd-of-models/. Accessed: 2024-11-10.

[5] NVIDIA. Nvidia nvl72, 2025. URL https://www.nvidia.com/en-us/data-center/gb200-nvl72/. Accessed: 2025-May-06.

[6] Rolf Neugebauer, Gianni Antichi, José Fernando Zazo, Yury Audzevich, Sergio López-Buedo, and Andrew W. Moore. Understanding pcie performance for end host networking. In *Proceedings of the 2018 Conference of the ACM Special Interest Group on Data Communication*, SIGCOMM '18, page 327–341, New York, NY, USA, 2018. Association for Computing Machinery. ISBN 9781450355674. doi: 10.1145/3230543.3230560. URL https://doi.org/10.1145/3230543.3230560.

[7] Celestial AI. Celestial AI, 2025. URL https://www.celestial.ai/. Accessed: 2025-05-14.

[8] HotChips 34. Passage—A Wafer-Scale, Programmable Photonic Communication Substrate. https://hc34.hotchips.org/assets/program/conference/day1, (Accessed on 2023-05-26).

[9] Kun Qian, Yongqing Xi, Jiamin Cao, Jiaqi Gao, Yichi Xu, Yu Guan, Binzhang Fu, Xuemei Shi, Fangbo Zhu, Rui Miao, Chao Wang, Peng Wang, Pengcheng Zhang, Xianlong Zeng, Eddie Ruan, Zhiping Yao, Ennan Zhai, and Dennis Cai. Alibaba hpn: A data center network for large language model training. ACM SIGCOMM '24, page 691–706, New York, NY, USA, 2024. Association for Computing Machinery. ISBN 9798400706141. doi: 10.1145/3651890.3672265. URL https://doi.org/10.1145/3651890.3672265.

[10] Hong Liu, Ryohei Urata, Kevin Yasumura, Xiang Zhou, Roy Bannon, Jill Berger, Pedram Dashti, Norm Jouppi, Cedric Lam, Sheng Li, Erji Mao, Daniel Nelson, George Papen, Mukarram Tariq, and Amin Vahdat. Lightwave fabrics: At-scale optical circuit switching for datacenter and machine learning systems. In *Proceedings of the ACM SIGCOMM 2023 Conference*, ACM SIGCOMM '23, page 499–515, New York, NY, USA, 2023. Association for Computing Machinery. ISBN 9798400702365. doi: 10.1145/3603269.3604836. URL https://doi.org/10.1145/3603269.3604836.

[11] Google Cloud. Introducing Trillium TPU and AI Hypercomputer. https://cloud.google.com/blog/products/ai-machine-learning/introducing-cloud-tpu-v5p-and-ai-hypercomputer, 2024. Accessed: 2024-05-07.

[12] Aashaka Shah, Vijay Chidambaram, Meghan Cowan, Saeed Maleki, Madan Musuvathi, Todd Mytkowicz, Jacob Nelson, Olli Saarikivi, and Rachee Singh. TACCL: Guiding collective algorithm synthesis using communication sketches. In *20th USENIX Symposium on Networked Systems Design and Implementation (NSDI 23)*, pages 593–612, Boston, MA, April 2023. USENIX Association. ISBN 978-1-939133-33-5. URL https://www.usenix.org/conference/nsdi23/presentation/shah.

[13] Mohammad Shoeybi, Mostofa Patwary, Raul Puri, Patrick LeGresley, Jared Casper, and Bryan Catanzaro. Megatron-lm: Training multi-billion parameter language models using model parallelism. *CoRR*, abs/1909.08053, 2019. URL http://arxiv.org/abs/1909.08053.

[14] Tpu v4 documentation. https://cloud.google.com/tpu/docs/v4, 2023. Accessed on 2024-05-29.

[15] Rajeev Thakur, Rolf Rabenseifner, and William Gropp. Optimization of collective communication operations in mpich. *Int. J. High Perform. Comput. Appl.*, 19(1):49–66, feb 2005. ISSN 1094-3420. doi: 10.1177/1094342005051521. URL https://doi.org/10.1177/1094342005051521.

[16] Liangyu Zhao, Saeed Maleki, Ziyue Yang, Hossein Pourreza, Aashaka Shah, Changho Hwang, and Arvind Krishnamurthy. Forestcoll: Efficient collective communications on heterogeneous network fabrics, 2024.

[17] Paul Sack and William Gropp. Collective algorithms for multiported torus networks. *ACM Trans. Parallel Comput.*, 1(2), feb 2015. ISSN 2329-4949. doi: 10.1145/2686882. URL https://doi.org/10.1145/2686882.

[18] Nikhil Jain and Yogish Sabharwal. Optimal bucket algorithms for large mpi collectives on torus interconnects. In *Proceedings of the 24th ACM International Conference on Supercomputing*, pages 27–36, 2010.

[19] Paul Sack and William Gropp. Collective algorithms for multiported torus networks. *ACM Trans. Parallel Comput.*, 1(2), feb 2015. ISSN 2329-4949. doi: 10.1145/2686882. URL https://doi.org/10.1145/2686882.

[20] Woosuk Kwon, Zhuohan Li, Siyuan Zhuang, Ying Sheng, Lianmin Zheng, Cody Hao Yu, Joseph Gonzalez, Hao Zhang, and Ion Stoica. Efficient memory management for large language model serving with pagedattention. In *Proceedings of the 29th Symposium on Operating Systems Principles*, SOSP '23, page 611–626, New York, NY, USA, 2023. Association for Computing Machinery. ISBN 9798400702297. doi: 10.1145/3600006.3613165. URL https://doi.org/10.1145/3600006.3613165.

[21] Abhishek Vijaya Kumar, Arjun Devraj, Darius Bunandar, and Rachee Singh. Chip-to-chip photonic connectivity in multi-accelerator servers for ml, 2025. URL https://arxiv.org/abs/2501.18169.

[22] Nvidia NVLink. Nvidia NVLink and NVSwitch, 2021. https://www.nvidia.com/en-us/data-center/nvlink/.

[23] William M. Mellette, Rajdeep Das, Yibo Guo, Rob McGuinness, Alex C. Snoeren, and George Porter. Expanding across time to deliver bandwidth efficiency and low latency. In *17th USENIX Symposium on Networked Systems Design and Implementation (NSDI 20)*, pages 1–18, Santa Clara, CA, February 2020. USENIX Association. ISBN 978-1-939133-13-7. URL https://www.usenix.org/conference/nsdi20/presentation/mellette.

[24] Mohammad Al-Fares, Alexander Loukissas, and Amin Vahdat. A scalable, commodity data center network architecture. In *Proceedings of the ACM SIGCOMM 2008 Conference on Data Communication*, SIGCOMM '08, page 63–74, New York, NY, USA, 2008. Association for Computing Machinery. ISBN 9781605581750. doi: 10.1145/1402958.1402967. URL https://doi.org/10.1145/1402958.1402967.

[25] Saksham Agarwal, Arvind Krishnamurthy, and Rachit Agarwal. Host congestion control. In *Proceedings of the ACM SIGCOMM 2023 Conference*, ACM SIGCOMM '23, page 275–287, New York, NY, USA, 2023. Association for Computing Machinery. ISBN 9798400702365. doi: 10.1145/3603269.3604878. URL https://doi.org/10.1145/3603269.3604878.

[26] D. Clark. The design philosophy of the darpa internet protocols. In *Symposium Proceedings on Communications Architectures and Protocols*, SIGCOMM '88, page 106–114, New York, NY, USA, 1988. Association for Computing Machinery. ISBN 0897912799. doi: 10.1145/52324.52336. URL https://doi.org/10.1145/52324.52336.

[27] Jayashree Mohan, Amar Phanishayee, and Vijay Chidambaram. CheckFreq: Frequent, Fine-Grained DNN checkpointing. In *19th USENIX Conference on File and Storage Technologies (FAST 21)*, pages 203–216. USENIX Association, February 2021. ISBN 978-1-939133-20-5. URL https://www.usenix.org/conference/fast21/presentation/mohan.

[28] Taiwan Semiconductor Manufacturing Company (TSMC). Tsmc: Leading semiconductor manufacturing. https://www.tsmc.com, 2025. Accessed: 2025-01-31.

[29] Daniel Pérez López. Programmable integrated silicon photonics waveguide meshes: optimized designs and control algorithms. *IEEE Journal of Selected Topics in Quantum Electronics*, 26(2): 1–12, 2019.

[30] Daniel Pérez, Ivana Gasulla, and José Capmany. Programmable multifunctional integrated nanophotonics. *Nanophotonics*, 7(8):1351–1371, 2018.

[31] Eric Ding and Rachee Singh. Pipswitch: A circuit switch using programmable integrated photonics. In *Optical Fiber Conference (OFC 2025)*, 2025. URL https://arxiv.org/abs/2501.18136.

[32] Meta AI. Llama 3.2: Multilingual large language models, 2024. URL https://www.llama.com/. Accessed: 2025-1-20.

[33] Stephen Merity, Caiming Xiong, James Bradbury, and Richard Socher. Pointer sentinel mixture models, 2016.

[34] Ziheng Jiang, Haibin Lin, Yinmin Zhong, Qi Huang, Yangrui Chen, Zhi Zhang, Yanghua Peng, Xiang Li, Cong Xie, Shibiao Nong, Yulu Jia, Sun He, Hongmin Chen, Zhihao Bai, Qi Hou, Shipeng Yan, Ding Zhou, Yiyao Sheng, Zhuo Jiang, Haohan Xu, Haoran Wei, Zhang Zhang, Pengfei Nie, Leqi Zou, Sida Zhao, Liang Xiang, Zherui Liu, Zhe Li, Xiaoying Jia, Jianxi Ye, Xin Jin, and Xin Liu. MegaScale: Scaling large language model training to more than 10,000 GPUs. In *21st USENIX Symposium on Networked Systems Design and Implementation (NSDI 24)*, pages 745–760, Santa Clara, CA, April 2024. USENIX Association. ISBN 978-1-939133-39-7. URL https://www.usenix.org/conference/nsdi24/presentation/jiang-ziheng.

[35] Zhizhen Zhong, Manya Ghobadi, Alaa Khaddaj, Jonathan Leach, Yiting Xia, and Ying Zhang. Arrow: Restoration-aware traffic engineering. In *Proceedings of the 2021 ACM SIGCOMM 2021 Conference*, SIGCOMM '21, page 560–579, New York, NY, USA, 2021. Association for Computing Machinery. ISBN 9781450383837. doi: 10.1145/3452296.3472921. URL https://doi.org/10.1145/3452296.3472921.

[36] Rachee Singh, Manya Ghobadi, Klaus-Tycho Foerster, Mark Filer, and Phillipa Gill. Radwan: Rate adaptive wide area network. In *Proceedings of the 2018 Conference of the ACM Special Interest Group on Data Communication*, SIGCOMM '18, page 547–560, New York, NY, USA, 2018. Association for Computing Machinery. ISBN 9781450355674. doi: 10.1145/3230543.3230570. URL https://doi.org/10.1145/3230543.3230570.

[37] Rachee Singh, Nikolaj Bjorner, Sharon Shoham, Yawei Yin, John Arnold, and Jamie Gaudette. Cost-effective capacity provisioning in wide area networks with shoofly. In *Proceedings of the 2021 ACM SIGCOMM 2021 Conference*, SIGCOMM '21, page 534–546, New York, NY, USA, 2021. Association for Computing Machinery. ISBN 9781450383837. doi: 10.1145/3452296.3472895. URL https://doi.org/10.1145/3452296.3472895.

[38] Xin Jin, Yiran Li, Da Wei, Siming Li, Jie Gao, Lei Xu, Guangzhi Li, Wei Xu, and Jennifer Rexford. Optimizing bulk transfers with software-defined optical wan. In *Proceedings of the 2016 ACM SIGCOMM Conference*, SIGCOMM '16, page 87–100, New York, NY, USA, 2016. Association for Computing Machinery. ISBN 9781450341936. doi: 10.1145/2934872.2934904. URL https://doi.org/10.1145/2934872.2934904.

[39] Arjun Singh, Joon Ong, Amit Agarwal, Glen Anderson, Ashby Armistead, Roy Bannon, Seb Boving, Gaurav Desai, Bob Felderman, Paulie Germano, Anand Kanagala, Jeff Provost, Jason Simmons, Eiichi Tanda, Jim Wanderer, Urs Hölzle, Stephen Stuart, and Amin Vahdat. Jupiter rising: A decade of clos topologies and centralized control in google's datacenter network. *SIGCOMM Comput. Commun. Rev.*, 45(4):183–197, aug 2015. ISSN 0146-4833. doi: 10.1145/2829988.2787508. URL https://doi.org/10.1145/2829988.2787508.

[40] Leon Poutievski, Omid Mashayekhi, Joon Ong, Arjun Singh, Mukarram Tariq, Rui Wang, Jianan Zhang, Virginia Beauregard, Patrick Conner, Steve Gribble, Rishi Kapoor, Stephen Kratzer, Nanfang Li, Hong Liu, Karthik Nagaraj, Jason Ornstein, Samir Sawhney, Ryohei Urata, Lorenzo Vicisano, Kevin Yasumura, Shidong Zhang, Junlan Zhou, and Amin Vahdat. Jupiter evolving: transforming google's datacenter network via optical circuit switches and software-defined networking. In *Proceedings of the ACM SIGCOMM 2022 Conference*, SIGCOMM '22, page 66–85, New York, NY, USA, 2022. Association for Computing Machinery. ISBN 9781450394208. doi: 10.1145/3544216.3544265. URL https://doi.org/10.1145/3544216.3544265.

[41] Weiyang Wang, Moein Khazraee, Zhizhen Zhong, Manya Ghobadi, Zhihao Jia, Dheevatsa Mudigere, Ying Zhang, and Anthony Kewitsch. TopoOpt: Co-optimizing network topology and parallelization strategy for distributed training jobs. In *20th USENIX Symposium on Networked Systems Design and Implementation (NSDI 23)*, pages 739–767, Boston, MA, April 2023. USENIX Association. ISBN 978-1-939133-33-5. URL https://www.usenix.org/conference/nsdi23/presentation/wang-weiyang.

[42] William M. Mellette, Rob McGuinness, Arjun Roy, Alex Forencich, George Papen, Alex C. Snoeren, and George Porter. Rotornet: A scalable, low-complexity, optical datacenter network. In *Proceedings of the Conference of the ACM Special Interest Group on Data Communication*, SIGCOMM '17, page 267–280, New York, NY, USA, 2017. Association for Computing Machinery. ISBN 9781450346535. doi: 10.1145/3098822.3098838. URL https://doi.org/10.1145/3098822.3098838.

[43] Navid Hamedazimi, Zafar Qazi, Himanshu Gupta, Vyas Sekar, Samir R. Das, Jon P. Longtin, Himanshu Shah, and Ashish Tanwer. Firefly: A reconfigurable wireless data center fabric using free-space optics. In *Proceedings of the 2014 ACM Conference on SIGCOMM*, SIGCOMM '14, page 319–330, New York, NY, USA, 2014. Association for Computing Machinery. ISBN 9781450328364. doi: 10.1145/2619239.2626328. URL https://doi.org/10.1145/2619239.2626328.

[44] Min Yee Teh, Zhenguo Wu, Madeleine Glick, Sebastien Rumley, Manya Ghobadi, and Keren Bergman. Performance trade-offs in reconfigurable networks for hpc. *Journal of Optical Communications and Networking*, 14(6):454–468, 2022. doi: 10.1364/JOCN.451760.

[45] Min Yee Teh, Shizhen Zhao, Peirui Cao, and Keren Bergman. Enabling quasi-static reconfigurable networks with robust topology engineering. *IEEE/ACM Transactions on Networking*, 31 (3):1056–1070, 2023. doi: 10.1109/TNET.2022.3210534.

[46] Zhenguo Wu, Liang Yuan Dai, Ziyi Zhu, Asher Novick, Madeleine Glick, and Keren Bergman. Sip architecture for accelerating collective communication in distributed deep learning. In *2023 Optical Fiber Communications Conference and Exhibition (OFC)*, pages 1–3, 2023. doi: 10.1364/OFC.2023.W1G.1.

[47] Anthony Rizzo and Keren Bergman. Realizing pb/s io with silicon photonic chiplets. In *Optica Advanced Photonics Congress 2022*, page NeTu1D.1. Optica Publishing Group, 2022. doi: 10.1364/NETWORKS.2022.NeTu1D.1. URL https://opg.optica.org/abstract.cfm?URI=Networks-2022-NeTu1D.1.

[48] Mehrdad Khani, Manya Ghobadi, Mohammad Alizadeh, Ziyi Zhu, Madeleine Glick, Keren Bergman, Amin Vahdat, Benjamin Klenk, and Eiman Ebrahimi. Sip-ml: High-bandwidth optical network interconnects for machine learning training. In *Proceedings of the 2021 ACM SIGCOMM 2021 Conference*.

[49] Yawei Yin, Mingyang Zhang, Zuqing Zhu, and S. J. B. Yoo. Fragmentation-aware routing, modulation and spectrum assignment algorithms in elastic optical networks. In *Optical Fiber Communication Conference/National Fiber Optic Engineers Conference 2013*, page OW3A.5. Optica Publishing Group, 2013. doi: 10.1364/OFC.2013.OW3A.5. URL https://opg.optica.org/abstract.cfm?URI=OFC-2013-OW3A.5.

[50] Ravi Mahajan, Xiaoqian Li, Joshua Fryman, Zhichao Zhang, Srikant Nekkanty, Pooya Tadayon, James Jaussi, Sergey Shumarayev, Ankur Agrawal, Susheel Jadhav, Kumar Abhishek Sing h, Andrew Alduino, Sushrutha Gujjula, Chia-Pin Chiu, Thomas Nordstog, Kaveh J. Hosseini,

Sandeep Sane, Nitin Deshpande, Kemal Aygün, Arnab Sarkar, Priyanka Dobriyal, Suresh Pot hukuchi, Vanessa A. Pogue, and David Hui. Co-packaged photonics for high performance computing: Status, challenges and opportunities. *J. Lightwave Technol.*, 40(2):379–392, Jan 2022. URL https://opg.optica.org/jlt/abstract.cfm?URI=jlt-40-2-379.

[51] Ali Sadr and Anthony Chan Carusone. A monolithic microring modulator-based transmitter with a multiobjective thermal controller. *IEEE Open Journal of the Solid-State Circuits Society*, 4:340–350, 2024. doi: 10.1109/OJSSCS.2024.3507754.

[52] Chen Sun, Mark Wade, Michael Georgas, Sen Lin, Luca Alloatti, Benjamin Moss, Rajesh Kumar, Amir H. Atabaki, Fabio Pavanello, Jeffrey M. Shainline, Jason S. Orcutt, Rajeev J. Ram, Miloš Popović, and Vladimir Stojanović. A 45 nm cmos-soi monolithic photonics platform with bit-statistics-based resonant microring thermal tuning. *IEEE Journal of Solid-State Circuits*, 51 (4):893–907, 2016. doi: 10.1109/JSSC.2016.2519390.